

Beta decay of  $^{39}\text{Cl}$ 

G. Wang, E. K. Warburton, and D. E. Alburger  
*Brookhaven National Laboratory, Upton, New York 11973*  
 (Received 20 February 1987)

The  $\beta$  decay of  $^{39}\text{Cl}$ , produced in the  $^{37}\text{Cl}(t,p)^{39}\text{Cl}$  reaction at  $E_t=3.1$  MeV, has been investigated with a Ge-NaI(Tl) Compton-suppression  $\gamma$ -ray spectrometer. Nineteen  $\gamma$ -ray transitions were observed, including 10 previously known. Precision energy measurements were carried out on six of the strongest lines. In the proposed decay scheme a weak new  $\beta$ -ray branch is established to the 2950-keV level of  $^{39}\text{Ar}$ , and the populations of  $^{39}\text{Ar}$  levels at 2093 and 2433 keV are accounted for by  $\gamma$ -ray decays from higher excited states. Spin-parity assignments are given.

## I. INTRODUCTION

Only two previous studies<sup>1,2</sup> have been made of the  $\beta$  decay of the  $J^\pi = \frac{3}{2}^+$  ground state of  $^{39}\text{Cl}$  [ $T_{1/2} = 55.6(2)$  min (Ref. 3)], the more recent being that of Engelbertink, Warburton, and Olness in 1972. Samples produced in the  $^{37}\text{Cl}(t,p)^{39}\text{Cl}$  reaction at  $E_t=3.0$  MeV were measured<sup>2</sup> with Ge(Li) and NaI(Tl) detectors in singles and in coincidence. A decay scheme was proposed that included 10  $\gamma$ -ray transitions and involved six excited states of  $^{39}\text{Ar}$ . Among the unanswered questions was that  $\gamma$  rays of 2093 keV were observed, but that the formation of the  $\frac{5}{2}^-$  2093-keV level appeared to be too intense to be accounted for by first-forbidden  $\beta^-$  decay, and  $\gamma$ -ray feeding of this state was not observed.

Our interest in a reinvestigation of  $^{39}\text{Cl}(\beta^-)^{39}\text{Ar}$  was stimulated by calculations simultaneously underway on the structure of  $^{39}\text{Ar}$ , reported in the following article.<sup>4</sup> That work utilizes the recently developed spherical shell-model interaction SDPF which uses a full  $(2s, 1d, 1f, 2p)$  configuration space.<sup>5</sup> Since  $^{39}\text{Cl}$  has  $N, Z = 22, 17$  the allowed Gamow-Teller (GT) beta decay  $^{39}\text{Cl}(\beta^-)^{39}\text{Ar}$  (see Fig. 3) should be describable within the model space  $^{16}\text{O}(2s, 1d)^{21}(1f, 2p)^2$  and as such can be calculated with the SDPF interaction.

The first-forbidden  $\beta^-$  decay modes of  $^{39}\text{Cl}$  involve in lowest order transitions to states within the  $^{16}\text{O}(2s, 1d)^{22}(1f, 2p)^1$  configuration. The formalism necessary to calculate nonunique first-forbidden decays in the  $A \sim 40$  mass region was recently developed<sup>6</sup> for use with the SDPF interaction and interest in such decays from  $^{39}\text{Cl}$  was therefore aroused.

The present experimental work reveals further details of the  $^{39}\text{Cl}$  decay scheme, answers some of the previous questions, and forms the basis for comparison with the theoretical calculations.<sup>4</sup> As part of our ongoing program of precision  $\gamma$ -ray energy determinations (see, e.g., Refs. 5 and 7), such measurements were made for  $^{39}\text{Ar}$   $\gamma$  transitions via  $^{39}\text{Cl}(\beta^-)^{39}\text{Ar}$ .

## II. EXPERIMENTAL METHODS

Sources of  $^{39}\text{Cl}$  were produced in the  $^{37}\text{Cl}(t,p)^{39}\text{Cl}$  reaction at  $E_t=3.1$  MeV by Van de Graaff bombardment of  $\text{Ba}^{37}\text{Cl}_2$  targets enriched to 90.4% in  $^{37}\text{Cl}$ . The powder samples were deposited as a slurry on thick Ta backings, and the beam currents were generally  $\sim 150$  nA for 1 h. After bombardment, the powder was scraped off the Ta backing into a small plastic bottle and then transferred to the detector in a fixed geometry. The detector was a Ge-NaI(Tl) Compton-suppression spectrometer including an intrinsic Ge detector with an efficiency at 1.33 MeV of 30% relative to a  $7.65 \times 7.65$ -cm NaI(Tl) detector, and a resolution [full width at half maximum (FWHM)] of 2.0 keV at that energy.

To study the complete  $\gamma$ -ray spectrum, each bombardment was made on a fresh target and measurements were made in a pulse-height analyzer during four successive 1-h runs, each separately recorded on tape. Previously unobserved transitions could then be assigned to  $^{39}\text{Cl}$  decay partially on the basis of their decay rates. Results from different bombardments were combined after making small gain-shift corrections.

The  $\gamma$ -ray efficiency versus  $E_\gamma$  was measured with  $^{56}\text{Co}$  and  $^{152}\text{Eu}$  sources, following standard techniques. An important part of the analysis was to establish the  $\gamma$ -ray summing corrections in order to distinguish between real  $\gamma$ -ray transitions and the summing effects of strong cascade  $\gamma$  rays. At the two source-to-detector distances used, i.e.,  $d=7.0$  and  $14.0$  cm, a  $^{60}\text{Co}$  source was counted and the intensity of the 2506-keV sum peak was determined relative to the 1173- and 1333-keV photopeaks. At  $d=7.0$  cm the results were  $I_{\text{sum}}/I_{1173} = 2.60 \times 10^{-3}$  and  $I_{\text{sum}}/I_{1333} = 2.85 \times 10^{-3}$ , while at  $d=14.0$  cm we obtained  $I_{\text{sum}}/I_{1173} = 8.4 \times 10^{-4}$  and  $I_{\text{sum}}/I_{1333} = 9.3 \times 10^{-4}$ . Uncertainties in all of these ratios were less than  $\pm 5\%$ . Extrapolations from these values could be used to calculate the amounts of summing expected for various cascade pairs of  $\gamma$  rays in  $^{39}\text{Cl}$  decay.

TABLE I. Gamma-ray energies, relative intensities, and branching ratios (BR) in  $^{39}\text{Cl}(\beta^-)^{39}\text{Ar}$ .

$J_i^\pi$	$^{39}\text{Ar}$ level $E_i$ (keV)	$E_f$ (keV)	$E_\gamma$ (keV)	Intensity <sup>a</sup> (relative)	Present	BR (%) <sup>b</sup> Ref. 3	Adopted
$\frac{3}{2}^-$	1267.207(8)	0	1267.191(11) <sup>c</sup>	10000	100	100	100
$\frac{3}{2}^+$	1517.540(8)	1267	250.333(3) <sup>c</sup>	8630(300)	54.1(10)	54.1(12)	54.1(8)
		0	1517.498(10) <sup>c</sup>	7320(160)	45.9(10)	45.9(12)	45.9(8)
$\frac{5}{2}^-$	2092.749(20)	1267	825.533	1.7(8)	8.9(38)	3.9(8)	4.1(10)
		0	2092.738(30)	17.3(4)	91.1(38)	96.1(8)	95.9(10)
$(\frac{5}{2}^-, \frac{7}{2}, \frac{9}{2}^-)$	2342.2(2)	0	2342.1	<0.2		100	100
$\frac{1}{2}^+$	2358.282(11)	1518	840.775(25)	24.8(6)	5.2(2)	3(1)	5.1(4)
		1267	1091.056(8) <sup>c</sup>	451(9)	94.8(2)	97(1)	94.9(4)
		0	2358.205	<1	<0.2	<0.3	<0.2
$\frac{3}{2}^-$	2433.48(3)	1518	915.86(10)	1.0(7)	11(7)	5.3(15)	5.6(15)
		1267	1166.250(50)	5.71(46)	65(6)	70.7(9)	70.7(9)
		0	2433.488(80)	2.08(13)	24(3)	23.8(9)	23.7(9)
$\frac{7}{2}^-$	2481.49(13)	0	2481.41	<0.4		82.5(6)	82.5(6)
$(\frac{3}{2}, \frac{5}{2})^+$	2503.417(11)	2093	410.690(20)	17.9(4)	4.3(2)	<7	4.3(2)
		1518	985.861(9) <sup>c</sup>	390(7)	92.8(2)	94(2)	92.8(2)
		1267	1236.190(50)	11.2(5)	2.7(2)	6(2)	2.7(2)
		0	2503.275(70)	1.0(1)	0.24(3)	<0.3	0.24(3)
$(\frac{5}{2}^-, \frac{7}{2}, \frac{9}{2}^-)$	2523.74(17)	0	2523.65	<0.3		100	100
$\frac{3}{2}^-$	2631.56(15)	2093	538.6	<0.4		81(2)	81(2)
$\frac{11}{2}^-$	2651.1(3)	0	2651.0	<0.2		100	100
$\frac{5}{2}^-$	2755.5(3)	0	2755.4	<0.5		56.3(14)	56.3(14)
$\frac{1}{2}^+$	2829.935(20)	2632	198.38	<0.5	<0.5		<0.5
		2524	306.21	<0.3	<0.3	<0.5	<0.3
		2503	326.52	<3.0	<2.8	<1.1	<1.1
		2433	396.462(40)	8.2(3)	7.5(3)		7.5(3)
		2358	471.65	<1.5	<1.4	<7.0	<1.4
		1518	1312.360(20) <sup>c</sup>	46.9(11)	43.0(8)	46.3(13)	42.8(8)
		1267	1562.704(25)	53.5(12)	49.0(8)	58.7(13)	49.2(8)
		0	2830.22(40)	<0.3	<0.25	<1.3	<0.25
$(\frac{3}{2}^+, \frac{5}{2})$	2949.95(10)	2503	446.61(13)	2.56(50)	52(6)	51.4(10)	51.4(10)
		1518	1432.27(15)	2.40(30)	48(6)	48.6(10)	48.6(10)
$\frac{1}{2}^+$	3287.0(4)	1267	2019.7	<0.7		100	100

<sup>a</sup>Limits correspond to two standard deviations.<sup>b</sup>The adopted values for upper limits are the smaller of the two values.<sup>c</sup>Value from precision energy measurements.

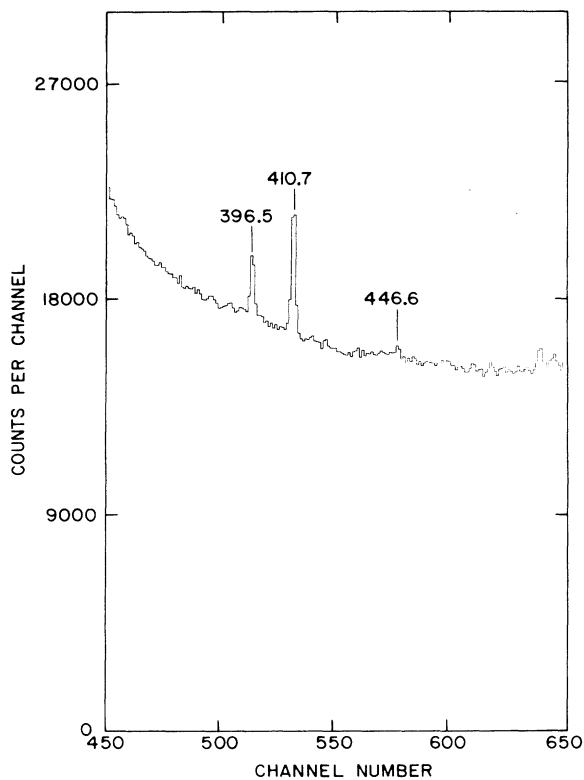


FIG. 1. Portion of the  $\gamma$ -ray spectrum from the decay of  $^{39}\text{Cl}$  showing newly observed  $\gamma$  rays of 396.5, 410.7, and 446.6 keV.

Precision energy measurements were made on six of the  $^{39}\text{Cl}$   $\gamma$  rays at high dispersion and with various digital offsets, following previously developed techniques.<sup>5,7</sup> Energy calibration sources included  $^{152}\text{Eu}$ ,  $^{22}\text{Na}$ ,  $^{110}\text{Ag}^m$ , and  $^{207}\text{Bi}$ . In addition to mixed-source runs, separate measurements on  $^{39}\text{Cl}$  and on each calibration source were made in order to check the individual spectra for weak  $\gamma$ -ray peaks that might occur in the vicinity of the lines being compared. In a given sequence of runs on a single source the precision  $E_\gamma$  measurements consisted of first comparing the  $\gamma$  rays in the 900–1500 keV range with the  $^{22}\text{Na}$ ,  $^{110}\text{Ag}^m$ , and  $^{207}\text{Bi}$  sources, in four or five runs of  $\sim 25$  min each, at various gain settings, and with a 6 mm thick Pb absorber in place. The absorber was then removed and another four or five runs of 25 min each were made comparing the 250-keV  $\gamma$  ray from  $^{39}\text{Cl}$  decay with the 244- and 344-keV  $\gamma$  rays from  $^{152}\text{Eu}$ . Results of the precision  $E_\gamma$  determinations, indicated in Table I, are each based on a total of 14–17 comparison measurements with the standard sources.

### III. RESULTS

#### A. Gamma-ray energies and branching ratios

Final data on the complete  $\gamma$ -ray spectrum were obtained at  $d = 7.0$  cm with three sources, measured for a combined total of 12 h. Portions of the summed spectrum are shown in Figs. 1 and 2. In Fig. 1 peaks are identified at 396.5, 410.7, and 446.6 keV that decay with the  $^{39}\text{Cl}$  half-life. They were not observed in the previous

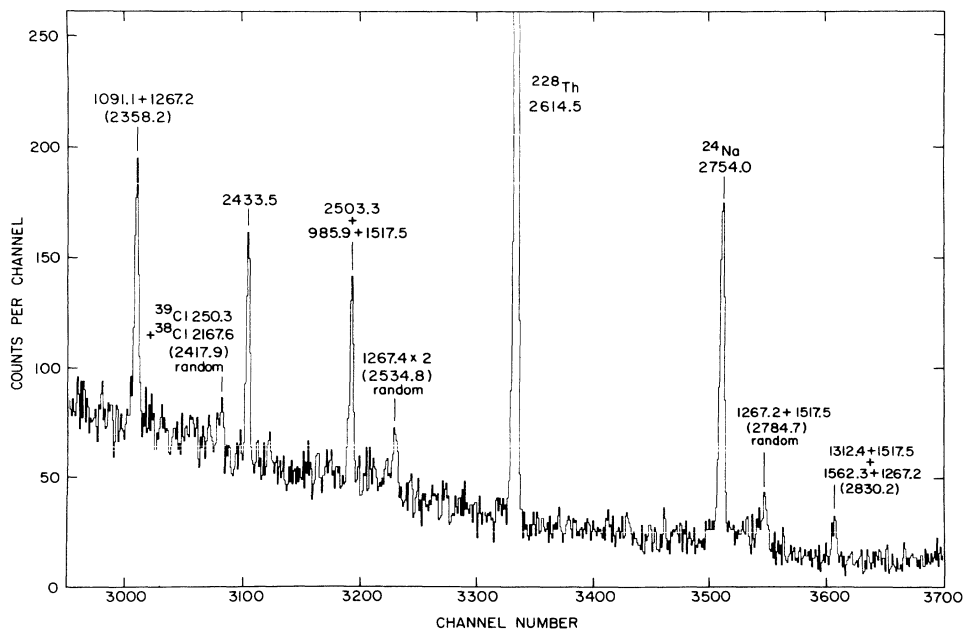


FIG. 2. Region of the  $^{39}\text{Cl}$   $\gamma$ -ray spectrum above 2.3 MeV. Various peaks (identified by their energies in keV) are discussed in the text.

TABLE II.  $\beta$ -ray branches,  $\log f_0 t$  values, and Gamow-Teller ( $B_0$ ) and unique first-forbidden ( $B_1$ ) transition strengths in the decay of  $^{39}\text{Cl}$  ( $J^\pi = \frac{3}{2}^+$ ).

$J^\pi$	$E_x$ (keV)	$\beta$ branch (%)	$\log f_0 t$	Order <sup>a</sup> ( $n$ )	$B_n^b$ ( $\text{fm}^{2n}$ )
$\frac{7}{2}^-$	0	7(2)	7.82(12)	1	1.3(4)
$\frac{3}{2}^-$	1267	4.5(16)	7.14(16)	nu	$f = 8.3(30) \times 10^{-2}$
$\frac{3}{2}^+$	1518	83.1(22)	5.65(2)	0	$13.74(6) \times 10^{-3}$
$\frac{1}{2}^+$	2358	2.56(5)	6.15(3)	0	$4.34(32) \times 10^{-3}$
$(\frac{3}{2}, \frac{5}{2})^+$	2503	2.24(4)	5.97(4)	0	$6.68(54) \times 10^{-3}$
$\frac{1}{2}^+$	2829	0.59(1)	5.84(5)	0	$8.85(97) \times 10^{-3}$
$(\frac{3}{2}, \frac{5}{2})$	2950	$26.6(32) \times 10^{-3}$	6.84(8)	0 <sup>c</sup>	$0.88(15) \times 10^{-3}$
$\frac{5}{2}^-$	2093	$< 8.6 \times 10^{-3}$	$> 8.9$	nu	$f < 1.6 \times 10^{-4}$
$(\frac{5}{2}, \frac{7}{2}, \frac{9}{2})^-$	2342	$< 1.2 \times 10^{-3}$	$> 9.5$	1, 2, or 3	$< 0.2^d$
$\frac{3}{2}^-$	2433	$< 6.2 \times 10^{-3}$	$> 8.6$	nu	$f < 1.1 \times 10^{-4}$
$\frac{7}{2}^-$	2481	$< 2.3 \times 10^{-3}$	$> 8.9$	1	$< 0.8$
$(\frac{5}{2}, \frac{7}{2}, \frac{9}{2})^-$	2523	$< 1.7 \times 10^{-3}$	$> 9.0$	1, 2, or 3	$< 0.8^d$
$\frac{3}{2}^-$	2631	$< 2.9 \times 10^{-3}$	$> 8.6$	nu	$f < 5.3 \times 10^{-5}$
$\frac{11}{2}^-$	2651	$< 1.2 \times 10^{-3}$	$> 8.9$	3	
$\frac{5}{2}^-$	2756	$< 5.2 \times 10^{-3}$	$> 8.1$	nu	$f < 9.6 \times 10^{-5}$
$\frac{1}{2}^+$	3287	$< 4.0 \times 10^{-3}$	$> 5.8$	0	$< 10 \times 10^{-3}$

<sup>a</sup>The degree of forbiddenness; nu denotes nonunique first forbidden.

<sup>b</sup>Allowed Gamow-Teller ( $n=0$ ) and first-forbidden unique ( $n=1$ ) transition strengths (matrix element squared).

<sup>c</sup>Assumed.

<sup>d</sup>This is the limit on  $B_1$  in the event that  $J^\pi = \frac{7}{2}^-$ .

work<sup>2</sup> because of the relatively high Compton continuum. In the region above 2.3 MeV, shown in Fig. 2, the numerous peaks have all been identified. The only real  $\gamma$  rays in the figure belonging to  $^{39}\text{Cl}$  decay are those at 2433.5 and 2503.3 keV. About half of the latter peak is actually due to  $985.9 + 1517.5$  summing at  $d=7.0$  cm. The net intensity of the real 2503.3-keV  $\gamma$  ray was confirmed in the run at  $d=14.0$  cm. Aside from the  $^{228}\text{Th}$  and  $^{24}\text{Na}$   $\gamma$  rays, all of the other peaks in Fig. 2 are due to either real or random summing of  $^{39}\text{Cl}$  (or in one case,  $^{39}\text{Cl} + ^{38}\text{Cl}$ )  $\gamma$  rays.

The results of the  $\gamma$ -ray measurements are summarized in Tables I and II and in the decay scheme of Fig. 3. We first consider Table I. Those  $E_\gamma$  with uncertainties attached are our measurements. Those without uncertainties were calculated from the level energies. Energies of levels from which  $\gamma$  decays were observed were calculated from a least squares fit to all measured  $\gamma$  energies assuming the level scheme of Fig. 3. Energies of levels for which no  $\gamma$  decay was observed are from Ref. 3. Limits on  $\gamma$ -ray intensities correspond to two standard deviations. The  $J^\pi$  assignments are from Ref. 3 or are discussed in the following paper.<sup>4</sup> There are no serious discrepancies with previous work. We observed nine  $\gamma$  rays not seen previously in  $^{39}\text{Cl}$   $\beta^-$  decay. The 447- and

1432-keV  $\gamma$  rays are associated with the decay of the  $^{39}\text{Ar}$  2950-keV level and the  $\beta$  branch to this level is the only new one resulting from this study. Three of the other seven new  $\gamma$  rays (i.e., 411, 826, and 2503 keV) represent new  $\gamma$  branches connecting  $^{39}\text{Ar}$  levels previously known to be fed by  $^{39}\text{Cl}$   $\beta^-$ . The 411-keV  $\gamma$  ray is assigned as  $2503 \rightarrow 2093$  and explains the bulk of the 2093-keV intensity, as discussed in the Introduction. The 826-keV  $\gamma$  ray is assigned as  $2093 \rightarrow 1267$ , and the 2503-keV transition is a weak ground-state decay. The remaining four new  $\gamma$  rays (i.e., 396, 916, 1166, and 2433 keV) are associated with the newly observed 396-keV  $2830 \rightarrow 2433$  transition and the subsequent decay of the 2433-keV level.

#### B. $\beta^-$ branching ratios, $\log ft$ values, and matrix elements

The  $\gamma$ -ray intensities of Table I and the decay scheme of Fig. 3 result in the  $\beta^-$  branching ratios of Table II. These branches result from the listed  $\gamma$  intensities of Table I with two exceptions. The poorly determined intensities for the  $2093 \rightarrow 1267$  and  $2433 \rightarrow 1518$  transitions were calculated from the intensities of the more intense branches and the adopted  $\gamma$ -ray branching ratios; i.e., use was made of previous information for these decay modes.

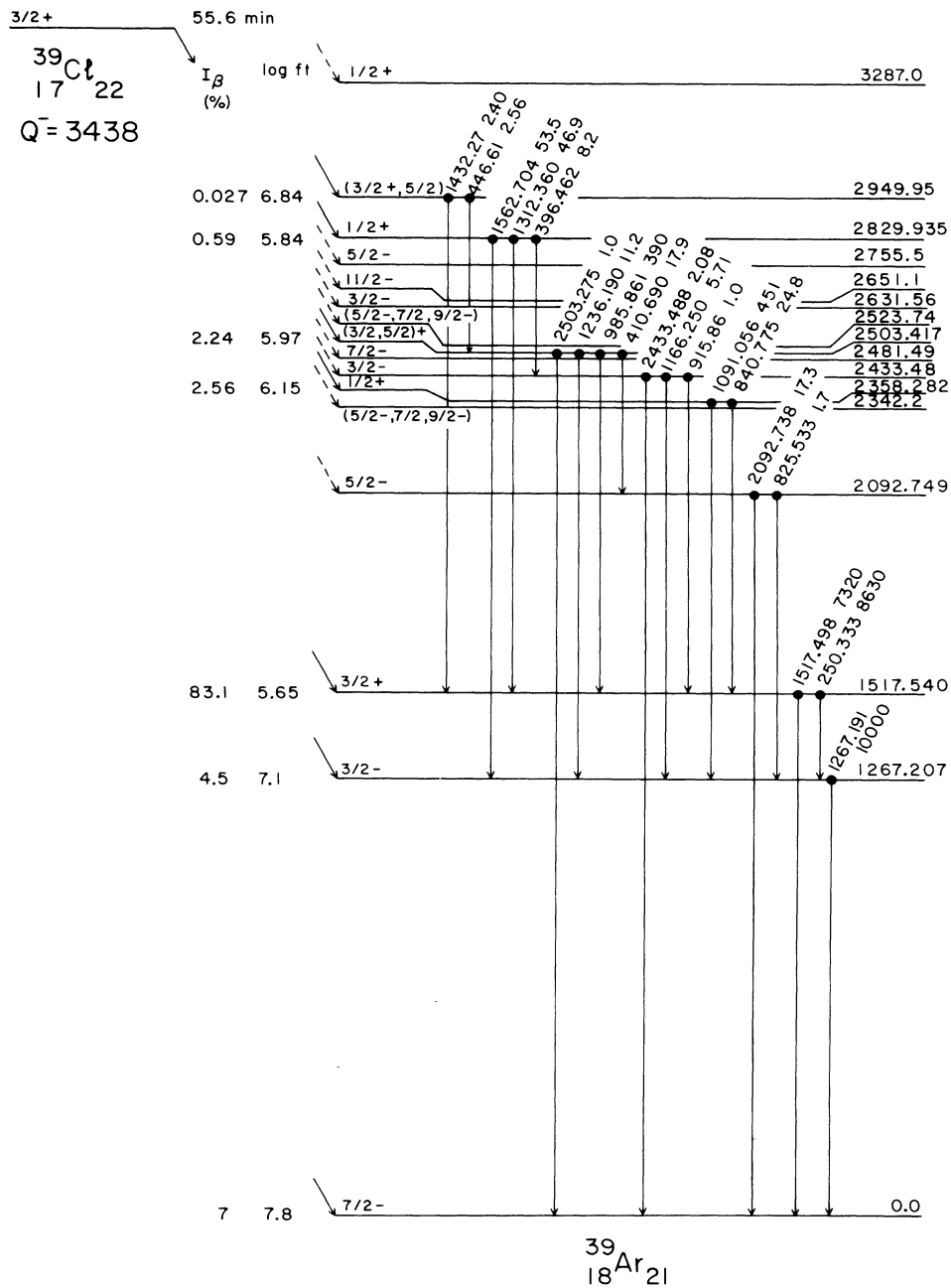


FIG. 3. Proposed decay scheme of  $^{39}\text{Cl}$ . All energies are in keV and  $\gamma$ -ray intensities are given relative to  $I_{1267\gamma} = 10000$ . For the  $^{39}\text{Ar}$  levels shown, but not directly fed in  $^{39}\text{Cl}$  decay,  $\beta$ -ray branching and  $\log ft$  limits are given in Table II.

The  $\beta^-$  branch into the ground state is from the work of Penning *et al.*<sup>1</sup>

The  $\log ft$  values of Table II were calculated assuming allowed decay,  $Q(\beta^-) = 3438(18) \text{ keV}$ ,  $T_{1/2} = 3336(12) \text{ s}$ , and the excitation energies of Table I.

The transition strengths (matrix element squared) for allowed Gamow-Teller ( $n=0$ ) and unique first-forbidden ( $n=1$ ) decay are defined by<sup>5</sup>

$$B_n = 6166 \left\{ \frac{[(2n+1)!!]^2}{(2n+1)} \right\} \lambda_{Ce}^{2n} (f_n t)^{-1}, \quad (1)$$

where  $2\pi\lambda_{Ce}$  is the Compton wavelength of the electron ( $\lambda_{Ce} = 386.159 \text{ fm}$ ). Equation (1) gives

$$B_0 = 6166/f_0 t, \quad 10^{-6} B_1 = 2758/f_1 t \text{ fm}^2, \quad (2)$$

where  $f_0$  and  $f_1$  are the Fermi functions calculated with shape factors of unity and  $\sim \frac{1}{12}(p^2+q^2)$ , respectively. For nonunique first-forbidden decay (designated by nu in column 5 of Table II) comparison to experiment is conventionally made via the  $f$  value, which is defined experimentally by  $f=6166/t_p$ , where  $t_p$  is the partial half-life

of the  $\beta^-$  branch in question (see Ref. 8).

A comparison of the experimental results with theoretical calculations is given in the following paper.<sup>4</sup>

This research was supported by the U. S. Department of Energy under Contract No. DE-AC02-76CH00016.

---

<sup>1</sup>J. R. Penning, H. R. Maltrud, J. C. Hopkins, and F. H. Schmidt, Phys. Rev. **104**, 740 (1956).

<sup>2</sup>G. A. P. Engelbertink, E. K. Warburton, and J. W. Olness, Phys. Rev. C **5**, 128 (1972).

<sup>3</sup>P. M. Endt and C. Van der Leun, Nucl. Phys. **A310**, 1 (1978).

<sup>4</sup>E. K. Warburton, Phys. Rev. C **35**, 2278 (1987), the following paper.

<sup>5</sup>E. K. Warburton, D. E. Alburger, J. A. Becker, B. A. Brown,

and S. Raman, Phys. Rev. C **34**, 1031 (1986).

<sup>6</sup>E. K. Warburton, D. J. Millener, B. A. Brown, and J. A. Becker, Bull. Am. Phys. Soc. **31**, 1222 (1986), and unpublished.

<sup>7</sup>E. K. Warburton and D. E. Alburger, Nucl. Instrum. Methods A **253**, 38 (1986).

<sup>8</sup>D. J. Millener, D. E. Alburger, E. K. Warburton, and D. H. Wilkinson, Phys. Rev. C **26**, 1167 (1982).